Deformation mechanism of high-density polyethylene probed by in situ Raman spectroscopy

Deformation mechanism of high-density polyethylene probed by *in situ* Raman spectroscopy

Takumitsu Kida

Tatsuya Oku

Yusuke Hiejima*

hiejima@se.kanazawa-u.ac.jp

Koh-hei Nitta

Department of Chemical and Materials Science, Kanazawa University, Kakuma Campus, Kanazawa 920-1192, Japan

*Corresponding author.

Abstract

The microscopic mechanism of high-density polyethylene under uniaxial drawing is investigated using *in situ* Raman spectroscopy. From the peak shifts of the symmetric and anti-symmetric C–C stretching modes, it is found that the load sharing on the polymer chain in the yielding region is anisotropic with stretching along the chain and compression perpendicular to the chain. The orientation functions ($\langle P_2 \rangle$ and $\langle P_4 \rangle$) as well as the orientation distribution function ($N(\theta)$) are determined from the polarized Raman spectra. The molecular orientation with cold drawing is found to proceed more effectively for lower crystallinity specimens. In the yielding region, it is also found that $N(\theta)$ has a maximum at the polar angle $\theta = 30–70°$. This peculiar behavior in the microscopic scale is explained by the preferential collapse of spherulites and the existence of lamellar clusters as the bulky mobile units.

Keywords: High-density polyethylene; *In situ* Raman spectroscopy; Mechanical properties

1 Introduction

Semi-crystalline polymers such as polyethylene (PE) and polypropylene (PP) show complicated morphologies composed of a mixture of crystalline and amorphous phases. The diversity in the structure with a wide range of length scales is responsible for the durability or high toughness of semi-crystalline polymers [1,2].

When a high-density polyethylene (HDPE) specimen is uniaxially drawn, the elastic deformation is followed by double yield points referred to as the first and the second yields. During such dual plastic deformations, large-scale transformation of the semi-crystalline morphology takes place, and collapse of the spherulite structures, necking of the sample specimens, and rearrangement of the lamellar crystals and the polymer chains have been observed [1–6]. Although various models, such as the lamellar local-melting and recrystallization model [4,7], and the lamellar cluster model [3,8–10], have been proposed for the deformation mechanism, such complicated changes in the hierarchical structures of semi-crystalline polymers are still controversial.

Spectroscopic techniques have been applied for the orientational behavior of PE during elongation [11–17]. The infrared (IR) spectroscopy has been applied intensively, and it has been established that the molecular chains in the crystalline and amorphous phases orientate toward the draw direction [11–14]. It has also been demonstrated that the orientation proceeds rapidly after the first yield, and gradually in the neck-propagation and the strain-hardening regions. However, the IR spectroscopy gives one orientation parameter $\langle P_2 \rangle$ which corresponds to the averaged orientation. For PE, the vibrations of the side chains, such as CH_2 twisting and wagging, are IR-active, and the skeletal vibrations of the C–C bonds are IR-inactive, then the load sharing on the polymer chains could not be directly observed with the IR spectroscopy.

Raman spectroscopy has several advantages to investigate the deformation behavior of polymeric materials [18–24]: it is applicable to opaque and thick samples, and molecular environments can be separately detected for both the crystalline and the amorphous phases. Raman scattering is an optical technique that provides a complementary approach to IR absorption when transparent and very thin (typically <100 μm thickness) films are required. In addition, it is advantageous to use Raman spectroscopy because the vibrations of the skeletal C–C bonds in main chains are directly observed [20,25]. Because the C–C stretching vibration is strongly Raman active, microenvironments of the polymer chains are probed by the spectral shifts [26,27]. Polarized Raman spectroscopy gives not only a measure of the average orientation, which is obtained by the usual spectroscopies such as birefringence and IR dichrom, but also the orientation distribution function (ODF, $N(\theta)$) [28–30]. In the yielding region where the neck of the specimen is formed, complicated deformation mechanism is expected. Indeed, various models for the plastic deformation of the crystalline chains have been proposed [1,3,4,8,27]. Two orientation parameters $\langle P_2 \rangle$ and $\langle P_4 \rangle$ given by the polarized Raman spectroscopy enable us to discuss the microscopic mechanism of deformation in detail.

Raman spectroscopy has been mainly applied off line for fibers and drawn specimens [31–34]. It should be emphasized that *in situ* measurements make it possible to provide transient data of the deformation behavior at the molecular level under tension, excluding the effects by stress relaxation that take place immediately after unloading the specimen. Recently, *in situ* Raman microscopy has been applied to PP films under uniaxial tensile testing, and the microscopic deformation mechanism has been discussed [27,35].

In this work, the deformation mechanism of HDPE in uniaxial tensile tests is investigated at the molecular level using *in situ* Raman spectroscopy. The load sharing and the orientation of the polymer chains are determined from the spectral changes with elongation. Based on these rheo-optical data, a novel molecular mechanism under uniaxial deformation is proposed.

2 Experimental

Ziegler–Natta–catalyzed HDPE samples supplied by Tosoh Corporation were used in this study. A sheet of HDPE with ~1 mm thickness was prepared by a hot-press method, where the pellets were melt at 210 °C for 5 min under compression at 20 MPa followed by quenching in iced water. The crystallinity of the sample was tuned with annealing temperatures from 40 to 110 °C at a fixed annealing time of 5 h. The test specimens for the measurements were cut out with a notch-shaped die (2 mm gauge length and 4 mm width) from the annealed film. The volumetric crystallinity of the sample was determined by the Archimedes method, where the density of the amorphous and the crystalline phases were assumed to be $\rho_a = 855\ kg/m^3$ and $\rho_c = 1000\ kg/m^3$ [36], respectively. The resultant volumetric crystallinities along with the characteristics of the samples are listed in Table 1.

Table 1 Characteristics of samples.

Sample code	$M_w/10^4$	M_w/M_n	Annealing temp. (°C)	Density (kg m^{-3})	Crystallinity (vol.%)
HDPE68(5.2)	5.2	5.2	110	953	68
HDPE66(5.2)	5.2	5.2	100	948	66
HDPE62(5.2)	5.2	5.2	40	943	62
HDPE68(10)	10	5.9	110	953	68

A schematic diagram of the apparatus for the *in situ* Raman spectroscopic measurements under uniaxial tensile testing is shown in Fig. 1(a). The Raman spectra were collected in back scattering geometry. A 20 mW He–Ne laser (LASOS) was used as the excitation light source. The laser light was monochromated with a laser line filter, and irradiated into the notched portion of the specimen. The diameter of the laser spot was ~1 mm. The shape of the specimen and the laser spot were schematically illustrated in Fig. 1(b). When the specimen initiates necking in the yielding region, the unnecked portion, as well as the necked portion, would exist in the beam spot. We have carried out the measurements with a smaller beam spot (smaller than 0.5 mm diameter), and confirmed the results would not be affected by the spot size. From the IR imaging of the PE under neck formation [37], it has been found that the molecular orientation dose not proceed in the unnecked portion in the neck-formation region, and the orientation proceeds rapidly during the neck formation. Their results suggest that the effect by the unnecked portion would be negligible, even if the necked and unnecked portions coexists in the observed region (e.g. between A and B in Fig. 1(b)). A custom-made tensile machine with double-drawing mechanism was installed in the optical path, and the scattered light was collected in back scattering geometry. The experiments were conducted at 20 °C at an elongation speed of 1 mm/min. It should be noted that the excitation laser was kept spotted at the notched portion during drawing. The scattered light was collected with a concave mirror and collimated with a convex lens into the optical fiber through a Raman long-pass filter. An intensified charge-coupled device camera equipped with a monochrometer (PIXIS100 and SpectraPro 2300i, Princeton Instruments) was used as the detector. For polarized Raman spectroscopy, a pair of wire-grid polarizers was inserted as the polarizer and the analyzer. The non-polarized spectra were accumulated 10 times with an exposure time of 1 s. The polarized spectra were collected in *zz*, *yz*, and *yy* geometries and accumulated 10 times with an exposure time of 2 s.

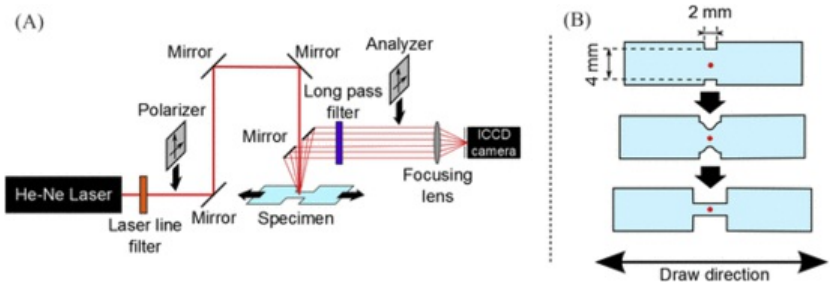

Fig. 1 Schematic illustrations of (a) experimental system for *in situ* Raman spectroscopy and (b) shape of the specimen and laser spot for undrawn (A), necking (B), and necked (C) samples.

A typical Raman spectrum in the C–C stretching region is shown in Fig. 2. The Raman bands of the C–C stretching modes in PE are listed in Table 2 [24,25,~~37,~~38,39]. The anti-symmetric (1063 cm^{-1}) and symmetric (1130 cm^{-1}) stretching modes correspond to the vibrations of carbon atoms along and perpendicular to the molecular chain, respectively. As shown in Fig. 2, the experimental Raman spectra were successfully fitted with a sum of two Voigt functions using a nonlinear Levenberg–Marquardt method, and the peak positions and the peak areas for the two peaks were determined. The uncertainties in determining the peak shifts and the peak areas were less than ±0.15 cm^{-1} and 4.0%, respectively. It should be noted here that the weak and broad peak at 1080 cm^{-1}, which was assigned to the C–C stretching in the amorphous phase, was safely ignored because the intensities of this band were sufficiently small because of the high crystallinity.

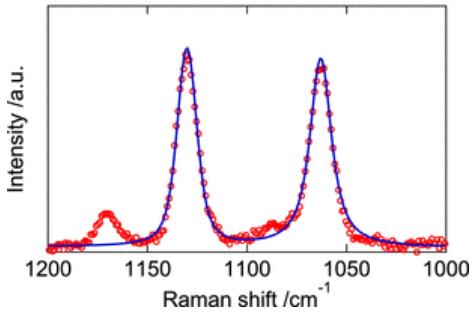

Fig. 2 Raman spectrum of undrawn HDPE68(5.2) (circles). The solid line is the fitting with a sum of two Voigt functions.

Table 2 Vibrational and phase assignments of the Raman spectrum of polyethylene.

Raman shift (cm^{-1})	Intensity	Mode[a]	Phase
1063	strong	ν_{as}(C–C)	Trans chain
1080	weak	ν(C–C)	Amorphous
1130	strong	ν_{s}(C–C)	Trans chain

[a] ν_s, symmetric stretching and ν_{as}, anti-symmetric stretching.

The positive and negative peak shifts were interpreted as the compressing and stretching stresses applied on the molecular chains, respectively. The peak shifts of the symmetric and anti-symmetric vibrations were defined as the deviation of the Raman shifts from that of the undrawn specimens:

$$\Delta\nu_s = \nu_s - \nu_s^0, \quad (1)$$

$$\Delta\nu_{as} = \nu_{as} - \nu_{as}^0, \quad (2)$$

where the superscript 0 denotes the undrawn specimens. From the direction of the symmetric and anti-symmetric vibrations, $\Delta\nu_s$ and $\Delta\nu_{as}$ were interpreted as the microscopic stresses perpendicular and parallel to the molecular chain, respectively.

The orientational behavior of main chains has been revealed by polarized Raman spectroscopy [16,28,~~39~~40–~~42~~43]. For PE, the symmetric C–C stretching mode at 1130 cm^{-1} is relevant. The integrated intensities of the polarized spectra are expressed as [20,29,~~39,~~40,41].

$$I_{yy} = b\left(\frac{8a^2+4a+3}{15} + \langle P_2\rangle\frac{8a^2-2a-6}{21} + 3\langle P_4\rangle\frac{a^2-2a+1}{35}\right), \quad (3)$$

$$I_{zz} = b\left(\frac{8a^2+4a+3}{15} - 2\langle P_2\rangle\frac{8a^2-2a-6}{21} + 8\langle P_4\rangle\frac{a^2-2a+1}{35}\right), \quad (4)$$

$$I_{yz} = b\left(\frac{a^2-2a+1}{15} - \langle P_2\rangle\frac{-a^2+2a-1}{21} - 4\langle P_4\rangle\frac{a^2-2a+1}{35}\right), \quad (5)$$

with

$$\frac{I_{yz}}{I_{zz}} = \frac{a^2-2a+1}{8a^2+4a+3}, \quad (6)$$

where I_{ij} denotes the integrated intensity for the *i*-polarized excitation and *j*-polarized scattered light. The terms *a* and *b* are associated with the principal elements of the polarizability tensor. In these equations, the orientation parameters $\langle P_2\rangle$ and $\langle P_4\rangle$ are written as a function of the chain orientation angle θ with respect to the draw axis as

$$\langle P_2\rangle = \frac{3\langle\cos^2\theta\rangle - 1}{2}, \quad (7)$$

$$\langle P_4\rangle = \frac{35\langle\cos^4\theta\rangle - 30\langle\cos^2\theta\rangle + 3}{8}. \quad (8)$$

The orientation parameters $\langle P_2\rangle$ and $\langle P_4\rangle$ are determined analytically by combining Eqs. (3)–(6). The value of $\langle P_2\rangle$ is an appropriate measure of the molecular orientation averaged over the entire direction [22,4344]. The upper and lower limits of $\langle P_2\rangle$ are 1 and −0.5, which correspond to a perfect alignment of the molecular chains along and perpendicular to the elongation direction, respectively. Combination with $\langle P_4\rangle$ enables discrimination of the difference in the possible orientation distributions even for identical $\langle P_2\rangle$ values [28,4041]. $\langle P_4\rangle$ has limiting values that depend on the specific $\langle P_2\rangle$ value, such that

$$\langle P_4\rangle_{\min} = \frac{1}{18}\left(35\langle P_2\rangle^2 - 10\langle P_2\rangle - 7\right) \le \langle P_4\rangle \le \frac{1}{12}\left(5\langle P_2\rangle + 7\right) = \langle P_4\rangle_{\max} \quad (9)$$

For a system with uniaxial symmetry, the polar angle distribution of polymer chains is described by the ODF ($N(\theta)$), which is expressed as an expansion of even Legendre polynomials ($P_l(\theta)$) [22,28]. For Raman spectroscopy, which gives $\langle P_2\rangle$ and $\langle P_4\rangle$, $N(\theta)$ is written as

$$N(\theta) = \frac{1}{2} + \frac{5}{2}\langle P_2\rangle P_2(\theta) + \frac{9}{2}\langle P_4\rangle P_4(\theta) \quad (10)$$

The fourth-order orientation parameter $\langle P_4\rangle$ enables the molecular orientation to be more precisely described, though a set of polarized Raman spectra with sufficiently high signal-to-noise ratios is required to determine the value of $\langle P_4\rangle$. To avoid the intrinsic difficulty in determining $\langle P_4\rangle$, Bower introduced the most probable distribution function, $\langle P_4\rangle_{mp}$, which is the calculated value of $\langle P_4\rangle$ for the given $\langle P_2\rangle$ with the maximum entropy assumption [28]. The expression for $\langle P_4\rangle_{mp}$ is

$$\langle P_4\rangle_{mp} = -0.083\langle P_2\rangle + 1.366\langle P_2\rangle^2 - 1.899\langle P_2\rangle^3 + 1.616\langle P_2\rangle^4 \quad (11)$$

for positive $\langle P_2\rangle$, and

$$\langle P_4\rangle_{mp} = 0.052\langle P_2\rangle + 1.574\langle P_2\rangle^2 + 3.968\langle P_2\rangle^3 + 8.058\langle P_2\rangle^4 \quad (12)$$

for negative $\langle P_2\rangle$ [29,4445]. In Fig. 3, $\langle P_4\rangle_{mp}$ is plotted against $\langle P_2\rangle$ (dashed line). Even if the value of $\langle P_2\rangle$ is fixed at zero, the orientation distribution function is not unique, as shown in Fig. 3(a)–(c); The random distribution corresponds to $\langle P_4\rangle = \langle P_4\rangle_{mp} = 0$, and the bimodal orientation at 0° and 90° and the unimodal orientation at 55° corresponds to $\langle P_4\rangle = \langle P_4\rangle_{max}$ and $\langle P_4\rangle = \langle P_4\rangle_{min}$, respectively.

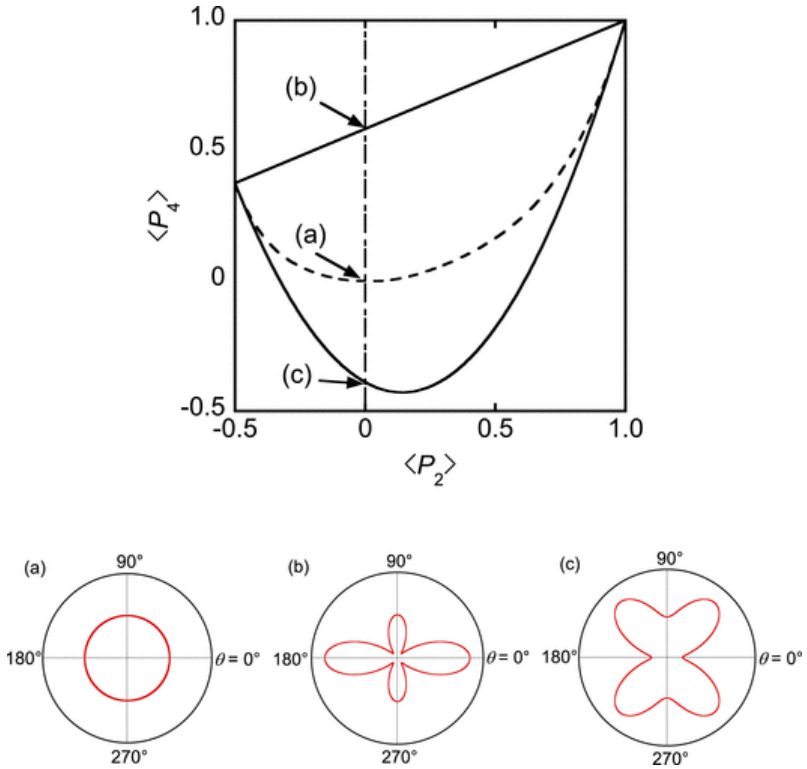

Fig. 3 $\langle P_2 \rangle$–$\langle P_4 \rangle$ diagram and a schematic representation of the different orientation distribution functions with $\langle P_2 \rangle = 0$.

3 Results

Fig. 4 shows the stress–strain curves of HDPE at 20 °C and elongation speed 1 mm/min. In the elastic region, the stress linearly increases with the applied strain. After the proportional region, the stress has a maximum at the first yield point ($\varepsilon = 0.6$) and the second yield point ($\varepsilon = 1.1$), at which the stress–strain curve has a slight hump and the test specimen initiates necking. Generally, the neck-propagation region is observed between and the yielding and the strain-hardening regions. However, since the present specimens have very short gauge (2 mm), the neck propagation completes in a narrow range (from $\varepsilon = 1.6$ to $\varepsilon = 2.0$), and the neck-propagation region is not clearly observed in the stress–strain curves. Beyond the yielding region with necking, the stress linearly increases with the applied strain in the strain-hardening region ($\varepsilon > 1.6$). It is obvious that higher crystallinity increases the overall stress level.

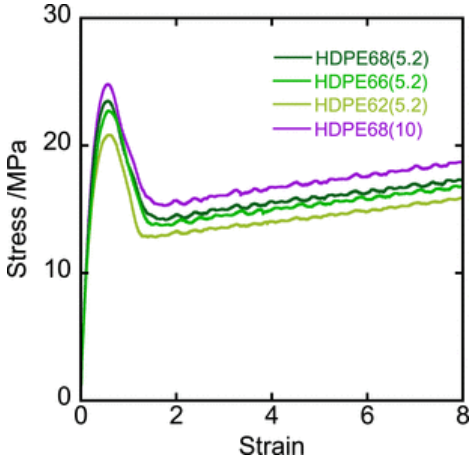

Fig. 4 Stress–strain curves of HDPE samples measured at 20 °C and elongation speed 1 mm/min.

In Fig. 5, *in situ* Raman spectra of HDPE68(5.2) at various strains are shown. Here, we focus on the two bands at 1130 and 1063 cm^{-1}. In Fig. 6, the peak shifts for the symmetric C–C stretching mode at 1130 cm^{-1} ($\Delta\nu_s$) are plotted against the applied strain. In the elastic region, $\Delta\nu_s$ remains zero irrespective of the crystallinity and molecular weight. At the first yield point ($\varepsilon = 0.6$), $\Delta\nu_s$ starts to increase with increasing strain, and has a maximum around the second yield point ($\varepsilon = 1.1$). In the strain-hardening region ($\varepsilon > 2$), the negative slope becomes gradual, and $\Delta\nu_s$ appears to approach an asymptotic value that depends on the crystallinity. In the strain-hardening region, because the peak shifts are more enhanced for the higher crystallinity HDPE and less dependent on the molecular weight, the load shearing on the polymer chains in the crystal phase is dominated by the crystallinity, and the higher crystallinity results in larger load shearing.

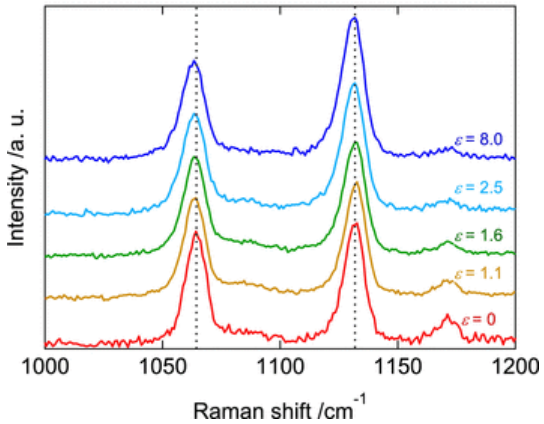

Fig. 5 *In situ* Raman spectra of HDPE68(5.2) at various strains.

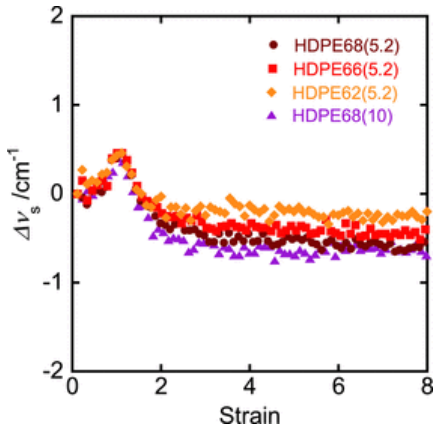

Fig. 6 Strain dependence of $\Delta\nu_s$ for HDPE68(5.2) (circles), HDPE66(5.2) (squares), HDPE62(5.2) (diamonds), and HDPE68(10) (triangles).

In Fig. 7, the strain dependence of the peak shifts for the anti-symmetric C–C stretching band at 1063 cm^{-1} ($\Delta\nu_{as}$) is shown. In the elastic region, $\Delta\nu_{as}$, as well as $\Delta\nu_s$, remains at zero, which suggests almost no stress is applied to the molecular chains in the crystalline phase. At the first yield point, $\Delta\nu_{as}$ starts to decrease, and gradually decreases with increasing strain. In the strain-hardening region, $\Delta\nu_{as}$ shows similar dependence on the crystallinity and the molecular weight to $\Delta\nu_s$.

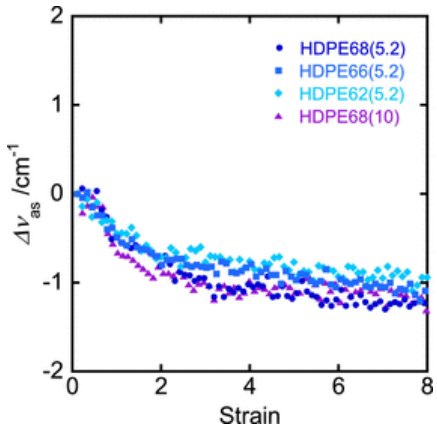

Fig. 7 Strain dependence of $\Delta\nu_{as}$ for HDPE68(5.2) (circles), HDPE66(5.2) (squares), HDPE62(5.2) (diamonds), and HDPE68(10) (triangles).

Except for $\Delta\nu_s$ in the yielding region, the peak shifts $\Delta\nu_s$ and $\Delta\nu_{as}$ are negative, indicating that the external stretching stresses on the polymer chain axis. It is quite reasonable that negative peak shifts are observed in the specimens under tensile stress. It should be emphasized that a distinct change in the load sharing occurs in the yielding region, because the load sharing on the polymer chain is anisotropic (stretching along the molecular chain and compression in the transverse direction on the chain axis), and the compression stress shows a maximum at the second yield point. For the peak shifts of highly oriented PE fibers [26], it has been demonstrated that both symmetric and anti-symmetric stretching modes show negative shifts under the load, and the peak shift for the anti-symmetric vibration is twice that of the symmetric vibration. In the present study, a similar relationship of $\Delta\nu_{as} \approx 2\Delta\nu_s$ was obtained in the strain-hardening region. A higher crystallinity sample shows greater peak shifts in the strain-hardening region, while $\Delta\nu_s$ and $\Delta\nu_{as}$ are less dependent on the molecular weight.

The polarized Raman spectra of HDPE68(5.2) at $\varepsilon = 8.0$ are shown in Fig. 8. The peak area of the 1130 cm^{-1} band strongly depends on the polarization, while the area of the 1063 cm^{-1} band depends little on the polarization. The larger peak area for the *zz* geometry suggests that the molecular chain is highly orientated along the draw direction at $\varepsilon = 8.0$.

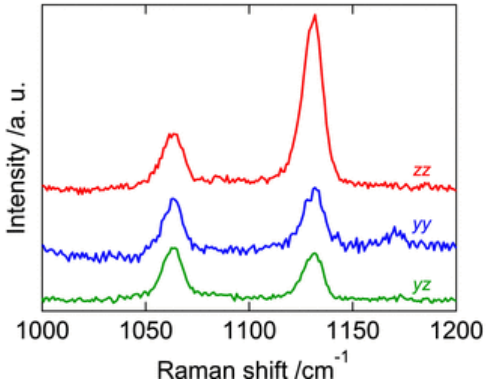

Fig. 8 *In situ* Raman spectra of HDPE68(5.2) at $\varepsilon = 8.0$ for various polarizations.

In Fig. 9, the orientation parameter $\langle P_2 \rangle$ is plotted against the applied strain. In the elastic region, $\langle P_2 \rangle$ remains close to zero irrespective of the applied strain. Beyond the first yield point, $\langle P_2 \rangle$ starts to increase and then rapidly increases with increasing strain. The slope then changes to gradually increasing in the strain-hardening region. This behavior suggests that orientation of the molecular chain in the elongation direction begins at the first yield point, proceeds rapidly up to the final stage of the second yield point, and then the highly orientated state is achieved in the strain-hardening region. These behaviors of $\langle P_2 \rangle$ are consistent with those estimated with the IR and the NIR spectroscopies [11–15]. It has been demonstrated that the orientation of the amorphous chains proceeds rapidly in the yielding region, as well as the crystalline chains, though the values of the orientation function of the amorphous chains are appreciably smaller than those of the crystalline chain [11–13,16,4243]. These orientational behaviors of the amorphous chains seem to be consistent with the present results for the crystalline chains. For HDPE with low crystallinity, the onset of the increase of $\langle P_2 \rangle$ takes place at slightly smaller strain and the slope of $\langle P_2 \rangle$ is slightly higher than for high crystallinity HDPE. The inverse dependence on crystallinity, where higher crystallinity leads to lower orientation, is associated with poor rearrangement of stacked crystalline blocks in the stretching direction. This is because the steric hindrance of the stacked crystalline blocks is enhanced by the increase of the rigid crystal structure within the blocks. No appreciable molecular-weight dependence is observed in the present study for the HDPE with relatively low molecular weights, which is consistent with IR and X-ray diffraction studies [37,46,47].

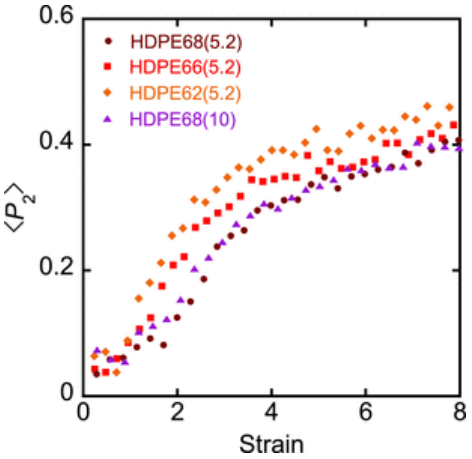

Fig. 9 Strain dependence of $\langle P_2 \rangle$ for HDPE68(5.2) (circles), HDPE66(5.2) (squares), HDPE62(5.2) (diamonds), and HDPE68(10) (triangles).

As shown in Fig. 10, $\langle P_4 \rangle$ remains almost constant at a slightly negative value in the initial elastic region. At the first yield point, $\langle P_4 \rangle$ begins to decrease with increasing strain, and has a shallow minimum in the early stage of strain hardening. Then, $\langle P_4 \rangle$ gradually increases with increasing strain, approaching a slightly positive value. HDPE with low crystallinity exhibits larger $\langle P_4 \rangle$, which indicates a broader distribution of molecular orientation. These peculiar behaviors of $\langle P_4 \rangle$ are highlighted by considering the most probable distribution function $\langle P_4 \rangle_{mp}$ [22,28,29,4445]. In Fig. 11, $\langle P_4 \rangle_{mp}$ is compared with the experimental $\langle P_4 \rangle$. Because $\langle P_4 \rangle_{mp}$ is a polynomial function of $\langle P_2 \rangle$ (see Eqs. (11) and (12)), the decrease of $\langle P_4 \rangle$ in the yielding region could not be reproduced. It should be pointed out that the values of $\langle P_4 \rangle$ are much smaller than $\langle P_4 \rangle_{mp}$. From the functional form of the second and the fourth Legendre polynomials, it is obvious that smaller $\langle P_4 \rangle$ is an indication of a broader distribution of orientations.

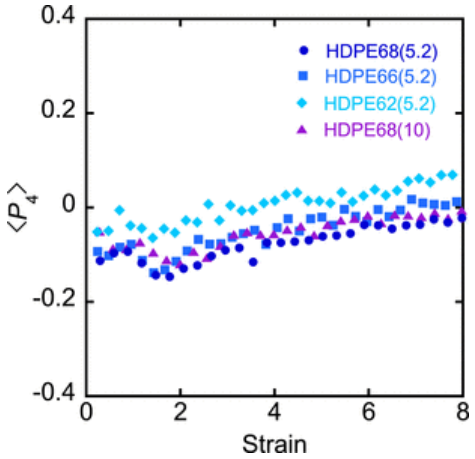

Fig. 10 Strain dependence of $\langle P_4 \rangle$ for HDPE68(5.2) (circles), HDPE66(5.2) (squares), HDPE62(5.2) (diamonds), and HDPE68(10) (triangles).

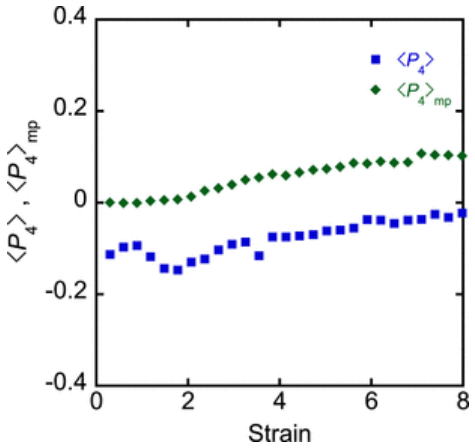

Fig. 11 Strain dependence of $\langle P_4 \rangle$ (squares) and $\langle P_4 \rangle_{mp}$ (diamonds) for HDPE68(5.2).

The experimental $\langle P_4 \rangle$ enables us to estimate $N(\theta)$. The functional forms of $N(\theta)$ for HDPE68(5.2) are shown in Fig. 12. From the definition, $N(\theta)$ of the undrawn sample has a constant value of 0.5. At the first yield point, the values of $N(\theta)$ increase in the polar direction ($\theta \approx 0°$) and decrease in the equatorial direction ($\theta \approx 90°$), which indicates the onset of molecular orientation. At the second yield point, while $N(\theta)$ in the equatorial direction further decreases, $N(\theta)$ in the polar direction remains almost constant. Moreover, $N(\theta)$ shows a broad peak in the intermediate direction (30–70°), which is a consequence of the negative deviation of $\langle P_4 \rangle$ in this region. After the second yield point, the peak at $\theta = 0$ becomes dominant, which indicates high orientation in the strain-hardening region. In the yielding region of semi-crystalline polymers, it has been demonstrated that the lamellar structure is partially collapsed, and the reorientation of polymer chains is attained through reordering of the lamellar crystal fragments (lamellar clusters) [8,10,4548]. The maximum of $N(\theta)$ in the intermediate direction may be because of the restructuring of the bulky lamellar clusters. Since $N(\theta)$ is calculated by using a set of $\langle P_2 \rangle$ and $\langle P_4 \rangle$, it should be emphasized that $N(\theta)$ could not be determined by the IR spectroscopy, and that these peculiar behaviors of $N(\theta)$ are highlighted by using a series of *in situ* measurements during tensile testing.

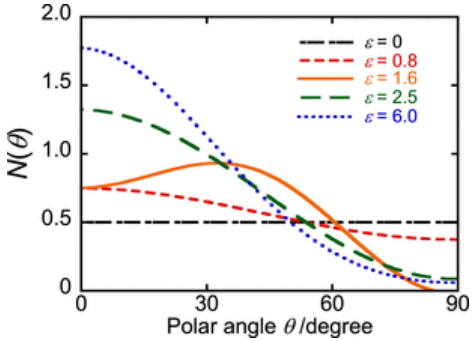

Fig. 12 Orientation distribution functions $N(\theta)$ of HDPE68(5.2) at various strains.

4 Discussion

The deformation mechanism of HDPE is schematically illustrated in Fig. 13. In the elastic region (ε = 0–0.6), where the stress linearly increases with increasing strain, the load sharing and the orientation parameters essentially remain zero. In this region, the spherulite structure elastically deforms (shown as an ellipse in Fig. 13), and there is little load sharing on the crystalline phase, suggesting that the stress concentrated on the non-crystalline phase with lower modulus. Nitta et al. [5,6] theoretically showed that the inter-lamellar molecular chains are stretched in the equatorial zone and compressed in the polar zone within affinely deformed spherulites.

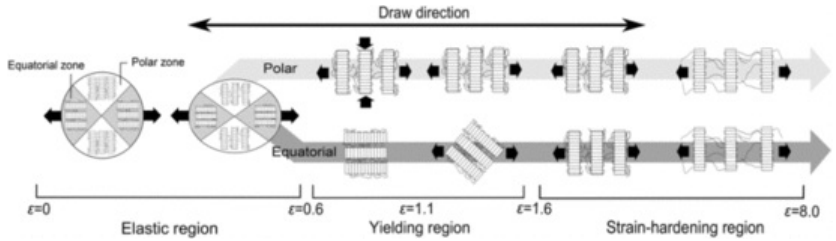

Fig. 13 Schematic illustration of the HDPE deformation mechanism.

In the yielding region (ε = 0.6–1.6), because the increase of $\langle P_2 \rangle$ is small (~0.1), the molecular orientation should only slightly occur. Then, the orientation of the crystals still remains essentially the same as in the elastic region. In the polar zone of a spherulite, because the polymer chains have already oriented along the draw direction, the stretching stress would be applied along the polymer chain. In the equatorial zone, because the polymer chains have directed perpendicular to the draw axis, the slight increase of $\langle P_2 \rangle$ is mainly because of the reorientation of the polymer chain in this zone. Fragmentation of the stacked crystalline lamellae (lamellar clusters) into cluster units within the collapsed spherulitic structure occurs at the first yield point. The fragmented lamellar cluster units behave as deformation units in the post first-yielding region, and then molecular reorientation is attained through the rotation of the lamellar cluster units. Because the lamellar cluster units are considered to be rigid and bulky cubic blocks [3], the rotational motions of the cluster units induce compression stress. Densification of the lamellar cluster units has been observed between the first and second yield [3]. Because compression stress perpendicular to the polymer chain is observed, the stress in the yielding region is concentrated on the crystals in the polar zone, and the anisotropy of the stress is induced by the densification of lamellar cluster units.

After the second yield point, $\Delta\nu_s$ sharply decreases and $\langle P_2 \rangle$ exponentially increases. The onset of the orientation of the crystals may reduce the compression stress on the polymer chain. $N(\theta)$ showed a maximum at an intermediate angle (30–70° from the elongation direction) and decreases in the perpendicular zone ($\theta \approx 90°$). This indicates that lamellar cluster units in the equatorial zone that were orientated along the polar direction before deformation preferentially reordered. In addition, $N(\theta)$ remained the same in the elongation direction ($\theta \approx 0°$), indicating that the lamellar cluster units in the polar zone showed no orientation until the second yield. The reorientation in the lamellar cluster blocks as the mobile unit would be inhibited because of the existence of the surrounding lamellar cluster units, which cause partial orientation along θ = 30–70°. It is noteworthy that the orientational behavior depends on the crystallinity, but only slightly depends on the molecular weight. For HDPE with lower crystallinities, the long period is shorter, which makes the size of the lamellar clusters smaller and more mobile [3,~~46~~49], and then the enhanced orientation is because of the smaller size of the lamellar clusters as the mobile unit.

In the strain-hardening region, the stress and the molecular orientation of crystals gradually increase with strain. The decrease of both $\Delta\nu_s$ and $\Delta\nu_{as}$ showed that stretching stress was applied to the chain and perpendicular axes. These

present results for PE sheets in the strain-hardening region are consistent with the results of the peak shifts $\Delta\nu_s$ and $\Delta\nu_{as}$ for PE fibers [26], where the peak shifts of the symmetric and anti-symmetric vibrations linearly decreased with increasing strain, and the shift for the anti-symmetric vibration was twice that for the symmetric vibration. Then, the load sharing on the crystals in the strain-hardening region was suggested to be similar to that for fibril structures.

5 Conclusion

In situ Raman spectroscopy was used to elucidate the molecular mechanism of the uniaxial cold drawing of HDPE. The peak shift of the symmetric C–C stretching mode shows positive deviation in the yielding region and has a maximum at the second yield point, while the peak shift of the anti-symmetric vibration has negative values and decreases with elongation. The anisotropic stress in the yielding region is because of the partial collapse of the spherulites, where the lamellar crystal in the equatorial zone preferentially collapses. From the orientation parameter $\langle P_2 \rangle$, it is found that HDPE with lower crystallinity shows higher orientation. The values of $\langle P_4 \rangle$ are substantially smaller than the most probable distribution function $\langle P_4 \rangle_{mp}$, which suggests a relatively broad orientation distribution. The orientation distribution function $N(\theta)$ shows a broad maximum at an intermediate polar angle $\theta = 30$–$70°$ in the yielding region, otherwise $N(\theta)$ has a maximum along the elongation direction.

~~Uncited reference~~

~~[48]; [49].~~

Acknowledgments

The authors are grateful to Dr. Takashi Uneyama for providing the software for curve fitting. YH is thankful for the financial support by JSPS KAKENHI Grant Number 26410221.

References

[1]

I.M. Ward and J. Sweeney, Mechanical properties of solid polymers, 3rd ed., 2013, WILEY.

[2]

E.F. Oleinik, *Polym Sci Ser C* **45**, 2003, 17–117.

[3]

M. Kuriyagawa and K.-H. Nitta, *Polym Guildf* **52**, 2011, 3469–3477.

[4]

A. Peterlin, *J Mater Sci* **6**, 1971, 490–508.

[5]

K.-H. Nitta, *Comput Theor Polym Sci* **9**, 1999, 19–26.

[6]

K.-H. Nitta and M. Takayanagi, *J Mater Sci* **38**, 2003, 4889–4894.

[7]

R.G. Snyder, J.R. Scherer and A. Peterlin, *Macromolecules* **14**, 1981, 77–82.

[8]

K.-H. Nitta and M. Takayanagi, *J Macromol Sci Part B Phys* **42**, 2003, 107–126.

[9]

K.-H. Nitta and M. Takayanagi, *Polym J* **38**, 2006, 757–766.

[10]

K.-H. Nitta and M. Takayanagi, *J Polym Sci Part B Polym Phys* **38**, 2000, 1037–1044.

[11]

B. Read and R. Stein, *Macromolecules* **1**, 1968, 116–126.

[12]

U. Hoffmann, F. Pfeifer and S. Okretic, *Appl Spectrosc* **47**, 1993, 1531–1539.

[13]

W. Glenz and A. Peterlin, *J Polym Sci Part A-2* **9**, 1971, 1191–1217.

[14]

N. Everall, J. Chalmers and P. Mills, *Appl Spectrosc* **50**, 1996, 1229–1234.

[15]

M. Mizushima, T. Kawamura, K. Takahashi and K. Nitta, *E-Polymers* **68**, 2012, 1618–1630.

[16]

J. Maxfield, R.S. Stein and M.C. Chen, *J Polym Sci Part B Polym Phys* **16**, 1978, 37–48.

[17]

J.H. Nobbs, D.I. Bower and I.M. Ward, *J Polym Sci Polym Phys Ed* **17**, 1979, 259–272.

[18]

R. Meier, *Polymer* **43**, 2002, 517–522.

[19]

J.L. Koenig, *Appl Spectrosc* **4**, 1971, 233–306.

[20]

M. Pigeon, E.R. Prud'homme and M. Pezolet, *Macromolecules* **24**, 1991, 5687–5694.

[21]

M. Glotin and L. Mandelkern, *Colloid Polym Sci* **260**, 1982, 182–192.

[22]

M. Tanaka and R.J. Young, *J Mater Sci* **41**, 2006, 963–991.

[23]

F. Rull, A.C. Prieto, J.M. Casado, F. Sobron and H.G.M. Edwards, *J Raman Spectrosc* **24**, 1993.

[24]

M. Gall, P. Hendra and C. Peacock, *Polymer* **13**, 1972, 104–108.

[25]

M. Gall, P. Hendra, O. Peacock, M.E.A. Cudby and H.A. Willis, *Spectrochim Acta Part A Mol Spectrosc* **28A**, 1972, 1485–1496.

[26]

R.P. Wool and R.S. Bretzlaff, *J Polym Sci Part B Polym Physicsl* **24**, 1986, 1039–1066.

[27]

J. Martin, M. Poncot, J.M. Hiver, P. Bourson and A. Dahoun, *J Raman Spectrosc* **44**, 2013, 776–784.

[28]

D.I. Bower, *J Polym Sci PartA-2 Polym Phys* **19**, 1981, 93–107.

[29]

M. Richard-Lacroix and C. Pellerin, *Macromolecules* **46**, 2013, 5561–5569.

[30]

M. Tanaka and R. Young, *Macromolecules* **39**, 2006, 3312–3321.

[31]

P. Tarantili, A. Andreopoulos and C. Galiotis, *Macromolecules* **31**, 1998, 6964–6976.

[32]

C. Fagnano, M. Rossi, R. Porter and S. Ottani, *Polymer* **42**, 2001, 5871–5883.

[33]

J.A.H.M. Moonen, W.A.C. Roobers, R.J. Meier and B.J. Kip, *J Polym Sci Part B Polym Phys* **30**, 1992, 361–372.

[34]

K. Prasad and D. Grubb, *J Polym Sci Part B Polym Phys* **27**, 1989, 381–403.

[35]

J. Martin and S. Margueron, *Polym Eng Science* **50**, 2010, 138–143.

[36]

J. Brundrup, E.H. Immergut, E.A. Grulke, A. Abe and D.R. Bloch, Polymer Handbook, 4th ed., 1999.

~~**[37]** H. Li, W. Zhou, Y. Ji, Z. Hong, B. Miao, X. Li, et al., *Polymer* **54**, 2013, 972–979~~[37] H. Li, W. Zhou, Y. Ji, Z. Hong, B. Miao, X. Li, et al., *Polymer* **5**, 2013, 972-979. .

[38]

R.T. Bailey, A.J. Hyde, J.J. Kim and J. McLeish, *Spectrochim Acta Part A Mol Spectrosc* **33A**, 1977, 1053–1058.

[39]

J. Schachtschneider and R. Snyder, *Spectrochim Acta* **19**, 1963, 117–168.

[40]

M.J. Citra, D.B. Chase, R.M. Ikeda and K.H. Gardner, *Macromolecules* **28**, 1995, 4007–4012.

[41]

D.I. Bower, *J Polym Sci PartA-2 Polym Phys* **10**, 1972, 2135–2153.

[42]

J. Purvis, D.I. Bower and I.M. Ward, *Polymer* **14**, 1973, 398–400.

[43]

S.A. Gordeyev, G.Y. Nikolaeva, K.A. Prokhorov and P.P. Pashinin, *Proc SPIE* **4069**, 2000, 66–75.

[44]

I.M. Ward, Structure and properties of oriented polymers, 2nd ed., 1997, Springer.

[45]

M. Richard-lacroix and C. Petterlin, *Appl Spectrosc* **67**, 2013, 409–419.

[46]

M. Butler, A. Donald, W. Bras, G.R. Mant, G.E. Derbyshire and A.J. Ryan, *Macromolecules* **28**, 1995, 6383–6393.

[47]

M. Butler and A. Donald, *Macromolecules* **31**, 1998, 6234–6249.

[48]

M. Takayanagi, K.-H. Nitta and O. Kojima, *J Macromol Sci Part B* **42**, 2003, 1049–1059.

[49]

K.-H. Nitta and M. Kuriyagawa, *Polym J* **44**, 2011, 245–251.

Graphical abstract

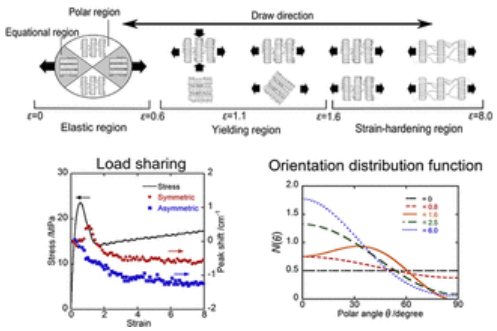

Highlights

- *In situ* Raman spectroscopy is applied to investigate the deformation mechanism of the uniaxial cold drawing of HDPE.
- ~~At the second yield point, t~~The load sharing ~~on the polymer chain~~in the yielding region is anisotropic with stretching along the polymer chain and compression perpendicular to the chain.
- In the yielding region, orientation distribution function shows a broad maximum in the intermediate direction (30–70°).

Queries and Answers

elsevier_JPOL_17488

Query: Highlights should only consist of 125 characters per bullet point, including spaces. The highlights provided are too long; please edit them to meet the requirement.

Answer: The second sentence is corrected.

Query: Please note that there is a mention of part figures ‘a’ and ‘b’ in the caption of ‘Fig. 1’ but there is no corresponding part figures provided in the artwork of ‘Fig. 1’. Kindly check and provide.

Answer: The revised version of Fig. 1 is provided by the attachment (Fig1.docx).

Query: This section comprises references that occur in the reference list but not in the body of the text. Please cite each reference in the text or, alternatively, delete it. Any reference not dealt with will be retained in this section.

Answer: Citations in the text are corrected.

Query: Please confirm that given names and surnames have been identified correctly.

Answer: OK.